ERROR ANALYSIS OF BOUNDARY CONDITIONS IN THE WIGNER TRANSPORT EQUATION

A Thesis
Presented to
The Academic Faculty

by

Timothy Philip

In Partial Fulfillment
of the Requirements for the Degree
Master of Science in the
School of Electrical and Computer Engineering

Georgia Institute of Technology
August 2014

ERROR ANALYSIS OF BOUNDARY CONDITIONS IN THE WIGNER TRANSPORT EQUATION

Approved by:

Paul D. Yoder, Advisor
School of Electrical and Computer Engineering
Georgia Institute of Technology

Azad J. Naeemi
School of Electrical and Computer Engineering
Georgia Institute of Technology

Benjamin D.B. Klein
School of Electrical and Computer Engineering
Georgia Institute of Technology

Date Approved: 01 July 2014

ACKNOWLEDGEMENTS

I would like to express my gratitude to my adviser Dr. P. Douglas Yoder for providing me the opportunity to research under him during my graduate and undergraduate careers. His guidance and mentorship have helped develop me into the researcher I am today, and I am forever grateful for his patience and understanding. I would also like to thank Dr. Azad Naeemi and Dr. Benjamin Klein for sitting on my committee and being accessible. Lastly, I would like to thank my friends, family, and Alexa for bearing with me throughout my Master's studies. This journey would have been far more difficult without the constant support I received.

TABLE OF CONTENTS

LIST OF FIGURES

SUMMARY

This work presents a method to quantitatively calculate the error induced through application of approximate boundary conditions in quantum charge transport simulations based on the Wigner transport equation (WTE). Except for the special case of homogeneous material, there exists no methodology for the calculation of exact boundary conditions. Consequently, boundary conditions are customarily approximated by equilibrium or near-equilibrium distributions known to be correct in the classical limit. This practice can, however, exert deleterious impact on the accuracy of numerical calculations and can even lead to unphysical results.

The Yoder group has recently developed a series expansion for exact boundary conditions which, when truncated, can be used to calculate boundary conditions of successively greater accuracy through consideration of successively higher order terms, the computational penalty for which is however not to be underestimated.

This thesis focuses on the calculation and analysis of the second order term of the series expansion. A method is demonstrated to calculate the term for any general device structure in one spatial dimension. In addition, numerical analysis is undertaken to directly compare the first and second order terms. Finally a method to incorporate the first order term into simulation is formulated.

CHAPTER I

INTRODUCTION

1.1 Simulation in Semiconductors

Since the invention of the transistor in 1947 and the development of the integrated circuit in 1958, microelectronics technology has developed at an astonishing rate [22]. Gate lengths of transistors rapidly shrank from 10 µm in the first MOSFET to 22 nm in modern processors. This miniaturization has allowed increasingly greater component density in circuits, which has enabled the high-volume, low-cost production of computers that has advanced fields ranging from telecommunications to medicine.

Much of this progress has been facilitated by the development of advanced theory and simulation. Because of the high cost involved with research, fabrication, and testing of such small components, the ability to accurate simulate device operation has been a vital tool in developing new designs. Simulation techniques involving the drift-diffusion equations and the Boltzmann transport equation (BTE) have been highly successful at modeling device operation and have given engineers tools for designing modern electronics.

1.2 Need for Quantum-based Simulation

As devices continue to scale down to nanometer dimensions, the classical theory that has driven the rate of current development fails to predict many effects. One notable example of this failure is in complementary metal-oxide-semiconductor (CMOS) transistors, the foundation of modern computers. In modeling the electrical behavior of CMOS transistors, the oxide between the gate electrode and the channel is generally assumed to block any DC current flow, which is valid for devices up to the micron

level. This assumption, however, fails in sub-micron and nanometer-scale transistors where electrons can "tunnel" through the thin gate oxide and generate appreciable current flow. This leakage current can degrade the performance of devices and ultimately limit the ability of transistors to scale further. Simulations based on classical physics fail to reproduce these quantum mechanical effects, rendering older simulation tools obsolete. Modern semi-classical simulations, however, try to incorporate quantum corrections to account for some effects to sufficient accuracy [4, 17].

As electronics continue to shrink further into the nanometer scale, however, quantum corrections to classical transport do not adequately model the device physics. Research into novel materials such as graphene or semiconductor heterostructures often requires full quantum mechanical descriptions to accurately understand device characteristics. In fact, many devices, such as the resonant tunneling diode, are explicitly designed to exploit quantum interactions for their operation [23].

Due to the nature of electronic transport as such small length scales, quantum mechanics can no longer be neglected or simply incorporated via corrections to classical physics. Fully quantum mechanical simulators are necessary for further development of electronic devices. Because of the complex interactions involved with electron interactions at the nanoscale, however, accurate and efficient simulations prove to be a challenge that requires strong understanding of the fundamental physics and mathematics of quantum mechanics.

1.3 Overview

In Chapter 2, some physical phenomena of quantum mechanics that exemplify the need for quantum simulations are described. The density matrix is then introduced as a method to analyze a statistical ensemble of particles as is necessary for devices with large numbers of electrons. Then using the density matrix, the phase-space Wigner function formalism is derived. Finally, the necessary steps to develop accurate

simulations using Newton's method to self-consistently solve for the Wigner function and the electrostatic potential are discussed. Chapter 3 details what an open quantum system is and why choosing accurate boundary conditions for numerical solutions poses a challenge. The error analysis series developed by the Yoder group is then introduced to as a way to aid in understanding of accurate boundary values. In Chapter 4, the second order term of the series is analytically simplified to a form more suitable for simulation purposes. The second order term in calculated in limiting cases to help elucidate the nature of both the second order term and the series in general. In Chapter 5, a scheme to numerically include the first term of the error series into device simulations is proposed.

CHAPTER II

QUANTUM CHARGE TRANSPORT THEORY

2.1 Quantum Mechanics

The development of quantum mechanics in the early twentieth century, sparked innovations in particle physics that changed the face of science. In his seminal 1927 work, Erwin Schrödinger proposed a mathematical description of the mechanics of electrons as waves [19]. This was eventually developed into his eponymous equation

$$\hat{H}\Psi = i\hbar\frac{\partial}{\partial t}\Psi, \tag{1}$$

where Ψ is the "wavefunction" that describes a single electron and $\hat{H}$ is the Hamiltonian operator that characterizes the energy of the electron. The nonrelativistic form of the Hamiltonian incorporated into Schrödinger's equation is given as

$$\left[-\frac{\hbar^2}{2m}\nabla^2 + V(\mathbf{r})\right]\Psi = i\hbar\frac{\partial}{\partial t}\Psi, \tag{2}$$

where $V(\mathbf{r})$ is the potential energy profile with which the electron interacts. The time-dependent Schrödinger's equation (TDSE) provides a probabilistic solution, or wavefunction, from which only expectation values of physical quantities can be determined. For example, the modulus squared of the wavefunction $|\Psi|^2$ provides a probability density function that can be integrated over space to determine the probability of an electron occupying a region. Other quantities are found by the use of various operators where an expectation value for an operator A is found by

$$\langle A\rangle = \int_{-\infty}^{\infty} \Psi A\Psi^* \, d\mathbf{r}. \tag{3}$$

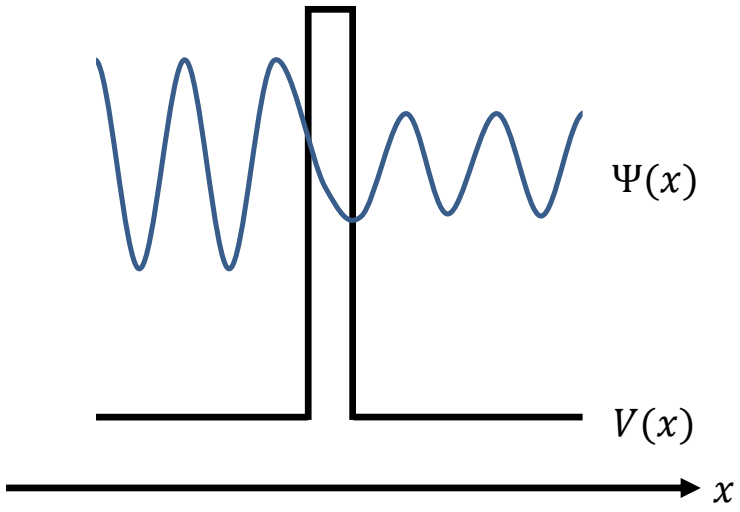

Figure 1: Depiction of electron tunneling through a thin potential barrier. Note that the wavefunction has finite amplitude on the right hand side of the barrier, implying that there is a probability that it exists on that side. Classically, an electron incident on such a barrier would be completely reflected.

Solving Eq. (2) for different potential energy structures and evaluating operators to compute physical observables helps scientists understand how electrons interact with their environment.

2.1.1 Electron Waves and Tunneling

When the potential energy profile is uniformly zero, the solutions for Eq. (2) are pure traveling plane waves, which is in stark contrast to classical descriptions of electrons, where they are described as discrete particles. This wave description allows for electrons to act in ways that classical particle descriptions would not allow. One example of a wave phenomenon in one dimension that Eq. (2) helps illuminate is that of an electron incident upon an energy barrier with finite width and height as shown in Figure 1.

Classically, an electron with kinetic energy less than the barrier height would completely reflect. Yet when Schrödinger's equation is solved for such a barrier, there

is a finite probability that the electron could tunnel through the barrier and reach the other side. The probability of transfer increases exponentially as the barrier becomes thinner and shorter. This idea of electron tunneling is key to understanding why leakage current became increasingly problematic as gate oxides became thinner in smaller transistors.

2.1.2 Energy Quantization

Solving the time-independent Schrödinger's equation (TISE) where temporal effects are neglected results in

$$\hat{H}\Psi_n = E_n\Psi_n \tag{4}$$

$$\left[-\frac{\hbar^2}{2m}\nabla^2 + V(\mathbf{r})\right]\Psi_n = E_n\Psi_n, \tag{5}$$

an eigenvalue equation where E_n is the energy eigenvalue of the electron. One illustrative example of a solution to the TISE is for that of the infinite quantum well in one dimension. The quantum well consists of a potential energy profile that is zero for a finite length L and infinite everywhere else as shown in Figure 2.

There are in fact an infinite number of solutions to the problem with varying integer index n, but more important than the individual solution is the energy associated with the nth solution of the problem

$$E_n = \frac{n^2\hbar^2\pi^2}{2mL^2}. \tag{6}$$

The possible values of energy are constrained or quantized to be exact values by Eq. (6), which deviates from the classical idea that electrons take on any of a continuous range of energies. The greater the confinement is, or in other words, the smaller L is, the farther the spacing between different possible energies. If L is allowed to be very large, the energy spacing becomes small and essentially continuous as one would expect in the classical limit.

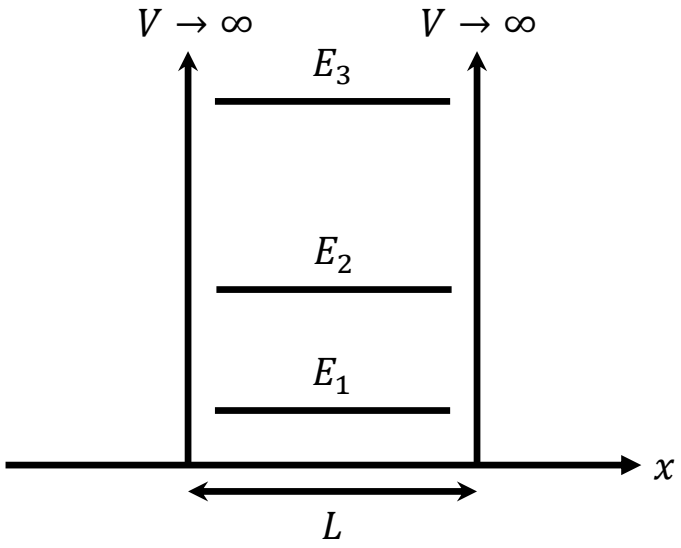

Figure 2: Potential energy profile of an infinite quantum well with width L. A few of the quantized energy states within the well are labeled with relative position indicting the value of energy.

Energy quantization is realized frequently in the design of semiconductor quantum well laser diodes. A thin layer of lower bandgap material is sandwiched between two materials of wider bandgap. This creates quantized energy levels in the well region that enhances the optical performance of the device.

2.2 Density Matrix

Although Schrödinger's equation and wave function operators are immensely useful for understanding the basics of quantum mechanics and single electron physics, it becomes cumbersome for dealing with large numbers of electrons as are present in most electronic devices. The density matrix ρ addresses this problem by tracking a statistical ensemble of electrons rather than a collection of wavefunctions of individual electrons [7].

The solutions provided by the TISE provide a basis on which any wavefunction can be written. In a thermally-distributed ensemble of electrons in equilibrium, the total wavefunction of their mixed state can be represented by a density matrix in the

form

$$\rho(\mathbf{r},\mathbf{r}') = \sum_n f^{(0)}(E_n)\psi_n^*(\mathbf{r})\psi_n(\mathbf{r}'), \tag{7}$$

where ψ_n is a basis function that satisfies Eq. (5) and $f^{(0)}(E_n)$ is the Fermi-Dirac distribution evaluated at the energy E_n related to the basis function. In this representation, the probability of occupation is determined by the diagonal elements of $\rho(\mathbf{r},\mathbf{r})$. More generally to describe non-equilibrium conditions with an arbitrary basis $\phi_i(\mathbf{r})$, the density matrix may be written as

$$\rho(\mathbf{r},\mathbf{r}') = \sum_m \sum_n c_{mn}\phi_m^*(\mathbf{r})\phi_n(\mathbf{r}'). \tag{8}$$

Here, off-diagonal elements represent correlations between different states. Regardless of the basis function used, the electron density can be calculated by

$$n(\mathbf{r}) = \rho(\mathbf{r},\mathbf{r}) = \sum_m \sum_n c_{mn}\phi_m^*(\mathbf{r})\phi_n(\mathbf{r}). \tag{9}$$

Limited to one dimension, the time evolution of the density matrix is governed by the quantum Liouville equation expressed as

$$\left[-\frac{\hbar^2}{2m}\left(\frac{\partial^2}{\partial x^2} - \frac{\partial^2}{\partial x'^2}\right) + V(x) - V(x')\right]\rho(x,x',t) = i\hbar\frac{\partial}{\partial t}\rho(x,x',t), \tag{10}$$

which can be directly derived from Schrödinger's equation [7].

2.3 Wigner Function Formalism

Eugene Wigner introduced a quantum-mechanical, phase-space distribution later named the Wigner distribution function (WDF), which is derived from the density matrix [24]. A phase-space representation of transport has advantages such as the calculation of statistical averages via integration in direct analogy to classical methods [14]. Whereas the density matrix only directly gives information about a single

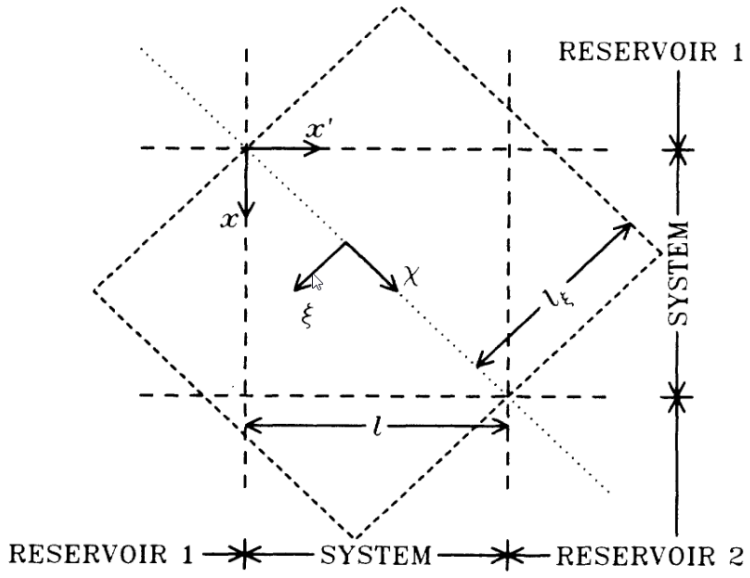

Figure 3: The Wigner function is based on different coordinates than the density matrix, the latter of which is based on x and x'. The center-of-mass coordinate χ is the average of the density matrix coordinates, and the difference coordinate ξ is based on the difference of the two coordinates. Image from [8]

representation at a time, a phase space distribution can also directly give physicists information about position and momentum, the latter of which is important for understanding current flow.

The WDF can be found directly from the density matrix by changing coordinates to center-of-mass coordinates χ and difference coordinates ξ as in Eq. (11) and Eq. (12). The difference between coordinates is illustrated in Figure 3.

$$\chi = \frac{1}{2}(x + x') \tag{11}$$

$$\xi = x - x' \tag{12}$$

The Liouville equation in Eq. (10) can then be written as

$$\left[-\frac{\hbar^2}{m}\left(\frac{\partial^2}{\partial\chi\partial\xi}\right) + V\left(\chi + \frac{\xi}{2}\right) - V\left(\chi - \frac{\xi}{2}\right)\right]\rho\left(\chi,\xi,t\right) = i\hbar\frac{\partial}{\partial t}\rho\left(\chi,\xi,t\right). \tag{13}$$

Next, the WDF f can be found by performing a spatial Fourier transform, referred to as the Wigner-Weyl transform, on the density matrix in the new coordinates [6]. For simplicity, the center-of-mass position variable will be replaced by the variable x because it is the principle position argument for the WDF. In one dimension, the WDF can be expressed as

$$f(x,k) = \frac{1}{2\pi\hbar} \int_{-\infty}^{\infty} e^{-ik\xi} \rho\left(x, \xi, t\right)\, d\xi. \tag{14}$$

Note that the the wave vector k is taken to be proportional to momentum by $\hbar$ in the effective mass approximation. Therefore, the Wigner function is taken to be a function of position and momentum. Care should be taken to understand that Heisenberg's principle is not violated despite position and momentum being independent variables. Measured quantities can only be interpreted as expectation values because the WDF is derived from the density matrix. The expectation value of a physical operator A can be found by the integrating across all wave vector as

$$\langle A \rangle \left(x,t\right) = \int_{-\infty}^{\infty} f(x,k,t) A(x,k,t)\, dk. \tag{15}$$

The electron density at a point in space can be evaluated as

$$\langle n \rangle \left(x,t\right) = \frac{1}{2\pi} \int_{-\infty}^{\infty} f(x,k,t)\, dk, \tag{16}$$

and electron flux density can be found as

$$\langle J \rangle \left(x,t\right) = \frac{\hbar}{2\pi m} \int_{-\infty}^{\infty} k f(x,k,t)\, dk. \tag{17}$$

2.3.1 Wigner Transport Equation

The power of the Wigner function approach comes from that fact that it does not have to be solved indirectly via Schrödinger's equation and Wigner-Weyl transforms. The

equation of motion for the WDF can be found by applying the Wigner-Weyl transform to Eq. (13). The resulting equation is called the Wigner transport equation (WTE) can be shown to be

$$\frac{\partial f(x,k,t)}{\partial t}+\frac{\hbar k}{m}\frac{\partial f(x,k,t)}{\partial x}+\frac{1}{2\pi\hbar}\int_{-\infty}^{\infty}V(x,k-k')f(x,k',t)\,dk'=\mathbb{C}f(x,k,t), \quad (18)$$

where f is the WDF and the mass m refers to the effective mass of a particle assuming parabolic dispersion [8]. The WDF interacts with the potential energy of the system $v(x)$ through the kernel of the third term of this equation, which is given as

$$V(x,k-k')=\int_{-\infty}^{\infty}\sin\left(\left(k-k'\right)\xi\right)\left[v\left(x+\frac{\xi}{2}\right)-v\left(x-\frac{\xi}{2}\right)\right]\,d\xi. \quad (19)$$

The potential operator describes the quantum interactions that take place due to potential energy variations throughout the device. The integration over space in Eq. (19) makes clear the nonlocal nature of these effects. In steady state, the WTE can be expressed as

$$\frac{\hbar k}{m}\frac{\partial f(x,k)}{\partial x}-\frac{2}{\pi\hbar}\int_{-\infty}^{\infty}\mathcal{I}m\left\{e^{2ik(x-\xi)}\int_{-\infty}^{\infty}f(x,k')e^{-2ik(x-\xi)}\,dk'\right\}v(\xi)\,d\xi=\mathbb{C}f(x,k). \quad (20)$$

The right hand side of Eq. (18) and Eq. (20) is a term called the collision operator and is added to account for scattering in the domain. The collision operator includes all mechanisms by which energy and momentum are exchanged between the system and its environment. Fully incorporating all of these effects proves to be difficult both analytically and numerically, and so a relaxation time approximation (RTA) given as

$$\mathbb{C}f(x,k,t)\approx-\frac{f(x,k)-f^{(0)}(k)}{\tau} \quad (21)$$

is often used. In the RTA, all loss mechanisms are described as the WDF relaxing to a known equilibrium or nonequilibrium distribution $f^{(0)}(k)$ over a characteristic time scale τ, which allows for simpler analysis and computation.

The resemblance of Eq. (18) to the well-known BTE has made the WTE a popular method for electronics software developers to enter into the quantum domain. Techniques such as Monte Carlo simulation that worked well with the BTE have had some success with the WTE but are ill-suited to describe sharp resonance peaks [16]. Additionally, a finite difference method has been established to solve directly for a discrete WDF [8]. The complex quantum interactions that are included in the WTE, however, create issues in simulations that are not seen with the BTE, especially in regard to electrically connecting devices to an external circuit.

2.3.2 Numerical Solution of the Stationary WTE

Analytic solutions to the WTE in Eq. (20) can only be solved for trivial potential profiles, so great interest has been brought forth for numerical techniques to simulate the equation [8]. The most common method is to use a second-order finite differencing scheme to solve for the discrete one-dimensional Wigner function [5].

Given N_x grid points in position and device length L, the grid spacing Δx can be shown to be equal to $L/(N_x - 1)$. Because of the Fourier relation between space and wave vector and the inherent periodicity of the the discrete Fourier transform, the values of wave vector are limited between positive and negative $\pi/2\Delta x$. Additionally, to aid the efficiency of numerical solution, it is best to avoid the a grid point where $k = 0$, which forces the wave vector grid spacing to $\Delta k = \pi/N_k\Delta x$ [8]. Therefore, the discretization grid in space x_j and momentum k_ℓ is

$$x_j = j\Delta x, \qquad j = 0, 1, \ldots N_x - 1 \tag{22}$$

$$k_\ell = \frac{\pi}{\Delta x}\left[\frac{1}{N_k}\left(\ell + \frac{1}{2}\right) - \frac{1}{2}\right], \qquad \ell = 0, 1, \ldots N_k - 1. \tag{23}$$

Discretizing the potential energy term of Eq. (20) takes special consideration because of the integration of the ξ variable. As Frensley noted, due to the nature of the derivation of the Wigner function, the values of ξ that are numerically integrated can

only be at multiples of $2\Delta x$ [8]. The interval of the ξ integration is constrained to an arbitrarily defined value of L_ξ, called the correlation length. This correlation length sets the distance about a point in space where quantum correlations and interactions are accounted. Although ideally infinite, the length chosen can impact simulation results and is discussed further in Chapter 3. Therefore, the discretization of the second term of Eq. (20) is

$$\frac{\Delta x \Delta k}{\pi \hbar} \sum_m \sum_p \left\{ \sin\left(\left(k_\ell - k_p \right) \xi_m \right) \left[v\left(x_j + \frac{\xi_m}{2} \right) - v\left(x_j - \frac{\xi_m}{2} \right) \right] \right\} f_{j,p}. \tag{24}$$

The first term of Eq. (20) can be discretized using by finite difference of the incoming and outgoing fluxes as

$$\left. \frac{\hbar k_\ell}{m} \frac{\partial f}{\partial x} \right|_{j,\ell} \approx \frac{1}{\Delta x} \left(F_{j+1/2,\ell} - F_{j-1/2,\ell} \right), \tag{25}$$

where the fluxes depend on the sign of the wave vector at that point [25]. The outgoing flux or the first term of the right hand side of Eq. (25) can be described by

$$F_{j+1/2,\ell} = \frac{\hbar k_\ell}{m} \left[\frac{1}{2}(f_{j,\ell} + f_{j+1,\ell}) + \frac{1-\kappa}{4} \left(-f_{j-1,\ell} + 2f_{j,\ell} - f_{j+1,\ell} \right) \right], \quad k_\ell > 0 \tag{26}$$

$$F_{j+1/2,\ell} = \frac{\hbar k_\ell}{m} \left[\frac{1}{2}(f_{j,\ell} + f_{j+1,\ell}) + \frac{1-\kappa}{4} \left(-f_{j,\ell} + 2f_{j+1,\ell} - f_{j+2,\ell} \right) \right], \quad k_\ell < 0. \tag{27}$$

The incoming flux or the second term of the right hand side of Eq. (25) can be described as

$$F_{j-1/2,\ell} = \frac{\hbar k_\ell}{m} \left[\frac{1}{2}(f_{j-1,\ell} + f_{j,\ell}) + \frac{1-\kappa}{4} \left(-f_{j-2,\ell} + 2f_{j-1,\ell} - f_{j,\ell} \right) \right], \quad k_\ell > 0 \tag{28}$$

$$F_{j-1/2,\ell} = \frac{\hbar k_\ell}{m} \left[\frac{1}{2}(f_{j-1,\ell} + f_{j,\ell}) + \frac{1-\kappa}{4} \left(-f_{j-1,\ell} + 2f_{j,\ell} - f_{j+1,\ell} \right) \right], \quad k_\ell < 0. \tag{29}$$

The variable κ in this four-point differencing scheme can be chosen to be to be any value between -1 and 1, but Yoder has shown that $\kappa = -1$, known as the one-sided upwind scheme, provides both accuracy and stability [25].

2.3.2.1 Self-consistency with Poisson's Equation

Because the Wigner function describes the movement of charges in a device and charge reorganization can influence the potential energy profile, it is necessary to solve Poisson's equation self-consistently with the WTE to generate accurate and physical results. Poisson's equation given as

$$\nabla \cdot \varepsilon(x) \nabla \phi(x) = -q[N_D(x) - n(x)] \tag{30}$$

governs the the relationship between the electrostatic potential ϕ, the ionized impurity concentration N_D, and the electron concentration n. The boundary conditions for this equation are determined both by applied bias V_{app} and any built in potentials due to band alignments ϕ_{bi}

$$\phi(0) = 0 \tag{31}$$

$$\phi(L) = \phi_{bi} + V_{app} \tag{32}$$

This equation can be discretized using a second-order central difference based on the same grid solved for in the WTE by

$$\frac{1}{\Delta x^2} \left[\varepsilon_{j+1}\phi_{j+1} - 2\varepsilon_j \phi_j + \varepsilon_{j-1}\phi_{j-1}\right] = q\left[N_{D,j} - n_j\right] \tag{33}$$

The electron density is a functional of the WDF as expressed by Eq. (16) and in the discrete case, can be approximated by

$$n_j = \frac{\Delta k}{2\pi} \sum_{\ell} f_{j,\ell}. \tag{34}$$

Using iterative methods to solve these equations self-consistently have produced accurate and efficient simulations [15].

2.3.2.2 Newton's Method for Self-consistency

Newton's method is used to self-consistently solve for the WDF and electrostatic potential. The method attempts to find the zeros of a nonlinear system of equations by using an initial guess and the derivative of the equations in respect to the solution variables at the same point to iteratively approach zero within a preset tolerance. To properly implement this method, the discrete Wigner and Poisson's equations must be rearranged to equate to zero. The Newton form of the discrete WTE equation for $\kappa = -1$ for the position x_j and wave vector k_ℓ is given as

$$\begin{aligned}&\frac{\hbar k_\ell}{2m\Delta x}\left[f_{j-2,\ell} - 4f_{j-1,\ell} + 3f_{j,\ell}\right] + \frac{1}{\tau}f_{j,\ell} - \frac{1}{\tau}f^{(0)}(k_\ell)\\ &-\frac{\Delta x \Delta k}{\pi\hbar}\sum_m\sum_p\left\{\sin\left(\left(k_\ell - k_p\right)\xi_m\right)\left[v\left(x_j + \frac{\xi_m}{2}\right) - v\left(x_j - \frac{\xi_m}{2}\right)\right]\right\}f_{j,p} = 0,\ k_l > 0\end{aligned} \tag{35}$$

$$\begin{aligned}&\frac{\hbar k_\ell}{2m\Delta x}\left[-3f_{j,\ell} + 4f_{j+1,\ell} - f_{j+2,\ell}\right] + \frac{1}{\tau}f_{j,\ell} - \frac{1}{\tau}f^{(0)}(k_\ell)\\ &-\frac{\Delta x \Delta k}{\pi\hbar}\sum_m\sum_p\left\{\sin\left(\left(k_\ell - k_p\right)\xi_m\right)\left[v\left(x_j + \frac{\xi_m}{2}\right) - v\left(x_j - \frac{\xi_m}{2}\right)\right]\right\}f_{j,p} = 0,\ k_l < 0\end{aligned} \tag{36}$$

$$v(x_m) = E_c(x_m) - q\phi(x_m), \tag{37}$$

and the Newton form of Poisson's equation based on Eq. (33) and Eq. (34) is

$$\frac{1}{\Delta x^2}\left[\varepsilon_{j+1}\phi_{j+1} - 2\varepsilon_j\phi_j + \varepsilon_{j-1}\phi_{j-1}\right] - qN_{D,j} + \frac{q\Delta k}{2\pi}\sum_\ell f_{j,\ell} = 0. \tag{38}$$

Note that equation Eq. (35) and Eq. (36) in total refer to $N_x \times N_k$ equations and Eq. (38) refers to N_x equations, which all must be solved self-consistently. Each row of the matrix represents one equation from the system, where each entry is a derivative in respect to the solution variable that corresponds to the column. This resulting matrix is referred to as the Jacobian matrix.

CHAPTER III

BOUNDARY CONDITIONS FOR THE WTE

Solutions of many differential equations such as the WTE are highly influenced by the spatial boundary conditions incorporated. As such, situations in the equations must be solved are often called boundary-value problems. Commonly solved quantum mechanical problems such as the infinite quantum well or the hydrogen atom have well-defined boundaries where the solution is known to approach a known value, usually zero. Electron devices involving current flow, however, require special treatment to accommodate the inflow and outflow of electrons from the active region [7].

3.1 Open Quantum Systems

A completely accurate description of the operation of a device would necessitate modeling not just the device but also the externally connected circuitry. Due to the multi-scale nature of quantum devices and their circuits, however, modeling this entire closed system proves to be analytically and numerically intractable. Therefore, it is imperative to be able to approach devices as open systems where the details of circuitry can be neglected.

An open quantum system is one that is designed such that a defined region can exchange particles with one or more large reservoirs of particles [9]. For device applications, this generally involves an active region with a characteristic potential energy profile that is is being studied, which is connected to two or more electrodes. These reservoirs in the leads can accommodate the inflow and outflow of electrons through the device allowing for a net current. Modeling contacts in semi-classical devices is well-understood [20], but the nature of quantum devices introduces considerations that can complicate accurate models.

Because of the nonlocal nature of quantum mechanics, boundary conditions to the WTE have been the subject of controversy [11, 12, 18, 21]. The potential term in Eq. (18) and Eq. (20) necessarily incorporates interactions between the electrical contacts at the boundary and the potential energy profile of the active region . In fact, the correlation length L_ξ from a given node inside the simulation domain can extend an appreciable distance into the reservoir regions as is illustrated in Figure 3. Therefore, the true boundary condition that is chosen at a contact must be a function of the a device's potential energy, and cannot be a predefined static value.

The problem can be circumvented by analyzing the behavior of the WDF in the contact regions. The WTE is known to simplify to the the BTE in the presence of polynomial potential energy profiles up to quadratic [2]. Because many quantum electronic devices contain long, homogeneous, and highly-conductive access regions between the electrodes and the active region, the electric field in these contact regions are approximately constant, which implies that the WDF in the contacts should approach the solution for the BTE for linear potentials. Therefore, the Wigner function far from potential energy discontinuities characteristic of an electronic device should be equal to the Fermi-Dirac distribution in equilibrium [8] or to a drifted Fermi-Dirac distribution for biases near equilibrium [14]. Using such distributions as boundary values at a finite distance often provides an adequate approximation for many device simulations [9, 25].

Because of this required level of approximation in the boundary conditions, however, numerical solutions of the WTE can still result in unphysical solutions such as negative electron densities. Some have cited these unphysical results as an intrinsic incompatibility of inflow boundaries and the WTE [21], but the origin of such results likely lies in an incompatibility of the boundary conditions with the specific potential profile used [13]. Some groups have proposed variations on traditional boundary conditions by modifying boundary conditions based on the potential energy profile [13]

or solving for adjustment parameters self-consistently with the simulation to adapt to device conditions [25]. These methods have shown promise in decreasing unphysical solutions and increasing the accuracy of simulations. Despite these advances, however, quantification of the error incurred through application of approximate boundary conditions for WTE simulations remains an unresolved issue in computational quantum electronics.

3.2 Application of Boundary Conditions in the WTE

The most common choice of boundary condition for the WTE is the equilibrium Fermi-Dirac distribution, which as noted previously provides an accurate approximation of the WDF in equilibrium far from any potential structures. Yoder *et al.* showed that the use of such equilibrium distributions are incompatible with current flow in nonequilibrium conditions and suggested the use of a drifted Fermi-Dirac distribution [25]. The drifted distribution integrated to one dimension is given as

$$f^{(0)}(k) = \frac{mk_BT}{\pi\hbar^2} \ln\left(1 + e^{-\frac{\hbar^2(k-\delta k)^2}{2mk_BT} + \frac{\mu}{k_BT}}\right), \tag{39}$$

where μ and T are the chemical potential and temperature of the reservoir, respectively. This distribution incorporates a drift parameter δk that must be self-consistently calculated with current flow by

$$\delta k = \frac{mJ}{\hbar n}, \tag{40}$$

where J and n are the current density the carrier density in the contact, respectively. Note that when the current is zero, the equilibrium Fermi-Dirac distribution is recovered as would be expected.

3.3 Error Analysis of Boundary Conditions

Although simulations with the WTE with approximate boundary conditions has effectively been used for predicting device behavior [8, 10, 14, 25], concerns regarding the error of results still exist. The error incurred by the use of such boundary values has been difficult to quantify because of the number of factors than can contribute to overall error in the WDF. The Yoder group, however, has successfully demonstrated a technique in which error specifically due to the application of boundary conditions can be evaluated for the stationary WTE [26].

To understand the effect of boundary conditions on the solution of the WTE, it becomes useful to define the Wigner propagator $\widehat{\mathcal{W}}$ based on Eq. (20) [21]. The WDF at any point in space can be found by applying the the Wigner propagator and adding it to a known reference value for the function at a position x_r through the expression

$$\begin{aligned} f(x,k) =& f(x_r,k) \\ &+ \int_{x_r}^{x} \left[\frac{2}{\pi\hbar^2 k} \int_{-\infty}^{\infty} \mathcal{I}m \left\{ e^{2ik(x-\xi)} \int_{-\infty}^{\infty} f(x,k') e^{-2ik(x-\xi)}\, dk' \right\} v(\xi)\, d\xi - \mathbb{C} f(x,k) \right] dx' \end{aligned} \tag{41}$$

$$f(x,k) = f(x_r,k) + \widehat{\mathcal{W}}(x,x_r) f(x,k). \tag{42}$$

Careful analysis using the Wigner propagator by the Yoder group has shown how the error due to approximate boundary conditions in simulation can contribute to global error [26]. Far from the active region, or as the reference position x_r approaches infinity, the WDF relaxes to an equilibrium or near-equilibrium distribution $f^{(0)}(k)$ in the RTA. Using that distribution as an approximate boundary condition a finite distance from the active region introduces error at a simulation boundary position x_b by the recursive equation in Eq. (42) and can be written as [26]

$$f(x_b,k) = \sum_{n=0}^{\infty} \widehat{\mathcal{W}}(x,k)^n f^{(0)}(k) \tag{43}$$

$$= f^{(0)}(k) + f^{(1)}(x,k) + f^{(2)}(x,k) + ... \tag{44}$$

The result in Eq. (44) implies that the true boundary value $f(x_b,k)$ is equal to the approximate condition $f^{(0)}(k)$ plus an infinite series of error terms. If successive terms are calculated and incorporated into the boundary condition, the boundary value will approach the numerically correct value for the given operating conditions.

3.3.1 First Order Correction Term

Some analytical simplification has been performed to facilitate understanding of the behavior of the first order term in this series. For any distribution $f^{(0)}(k)$ used as a boundary condition for the WTE, the first order error term can be calculated by [26]

$$f^{(1)}(x,k) = \left(\frac{2\tau}{\pi\hbar}\right) \int_{-\infty}^{\infty}\int_{-\infty}^{\infty} \frac{\sin\left(2\left(k-k'\right)\left(x-\xi\right)\right)}{1+4\left(k-k'\right)^2 {\ell_c}^2} v(\xi) f^{(0)}(k')\, d\xi dk' \\ - \left(\frac{2\tau}{\pi\hbar}\right) \int_{-\infty}^{\infty}\int_{-\infty}^{\infty} \frac{2\left(k-k'\right)\ell_c \cos\left(2\left(k-k'\right)\left(x-\xi\right)\right)}{1+4\left(k-k'\right)^2 {\ell_c}^2} v(\xi) f^{(0)}(k')\, d\xi dk', \tag{45}$$

where ℓ_c is given as $\frac{\hbar k\tau}{m}$, a quantum analogy to the mean free path. Eq. (45) simplifies the numerical integration necessary to incorporate the first order term into simulations without loss of generality.

CHAPTER IV

SECOND ORDER CORRECTION TERM

4.1 Development of Second Order Term

Analysis of successive terms of the Eq. (44) can quickly become difficult. The second order term can be be found by applying the Wigner propagator to the first order term from Eq. (45) due to the recursive nature of the series. Without any simplification, the expression for the second order term is expressed as

$$\begin{aligned} f^{(2)}(x,k) = \left(\frac{4\tau^2}{\pi^2\hbar^2\ell_c}\right) \int_{-\infty}^{\infty}\int_{-\infty}^{\infty}\int_{-\infty}^{\infty}\int_{-\infty}^{\infty} e^{-x/\ell_c} \int_{-\infty}^{x} e^{x'/\ell_c} \sin\left(2\left(k-k''\right)\left(x'-\xi'\right)\right) \\ \sin\left(2\left(k''-k'\right)\left(x'-\xi\right)\right)\ dx' \frac{v(\xi)f(k')v(\xi')}{1+4\left(k''-k'\right)^2\ell_c''^2}\ d\xi dk' d\xi' dk'' \\ + \left(\frac{4\tau^2}{\pi^2\hbar^2\ell_c}\right) \int_{-\infty}^{\infty}\int_{-\infty}^{\infty}\int_{-\infty}^{\infty}\int_{-\infty}^{\infty} e^{-x/\ell_c} \int_{-\infty}^{x} e^{x'/\ell_c} \sin\left(2\left(k-k''\right)\left(x'-\xi'\right)\right) \\ \cos\left(2\left(k''-k'\right)\left(x'-\xi\right)\right)\ dx' \frac{2\left(k''-k'\right)\ell_c''v(\xi)f(k')v(\xi')}{1+4\ell_c''^2\left(k''-k'\right)^2}\ d\xi dk' d\xi' dk'' \end{aligned} \tag{46}$$

where $\ell_c'' = \frac{\hbar\tau k''}{m}$. After applying the method of the integrating factor and integration by parts, one spatial integration can be analytically be simplified to reduce the integration to two in wave vector and two in position. This results in the following expression:

$$
\begin{aligned}
f^{(2)}(x,k) = \\
&\left(\frac{2\tau^2}{\pi^2\hbar^2}\right)\iiiint\left\{\frac{2\ell_c(k+k'-2k'')\sin\left[2(k+k'-2k'')x-2\left(k-k''\right)\xi'+2\left(k''-k'\right)\xi\right]}{\left(1+4{\ell_c}^2(k+k'-2k'')^2\right)}\right. \\
&\qquad+\frac{\cos\left[2(k+k'-2k'')x-2\left(k-k''\right)\xi'+2\left(k''-k'\right)\xi\right]}{\left(1+4{\ell_c}^2(k+k'-2k'')^2\right)} \\
&\qquad-\frac{2\ell_c(k-k')\sin\left[2(k-k')x-2\left(k-k''\right)\xi'-2\left(k''-k'\right)\xi\right]}{\left(1+4{\ell_c}^2(k-k')^2\right)} \\
&\qquad\left.-\frac{\cos\left[2(k-k')x-2\left(k-k''\right)\xi'-2\left(k''-k'\right)\xi\right]}{\left(1+4{\ell_c}^2(k-k')^2\right)}\right\} \\
&\qquad\qquad\frac{v(\xi)f^{(0)}(k')v(\xi')}{\left(1+4\ell_c''^2\left(k''-k'\right)^2\right)}\,d\xi dk' d\xi' dk'' \\
&+\left(\frac{2\tau^2}{\pi^2\hbar^2}\right)\iiiint\left\{\frac{\sin\left[2(k+k'-2k'')x-2\left(k-k''\right)\xi'+2\left(k''-k'\right)\xi\right]}{\left(1+4{\ell_c}^2(k+k'-2k'')^2\right)}\right. \\
&\qquad+\frac{2\ell_c(k+k'-2k'')\cos\left[2(k+k'-2k'')x-2\left(k-k''\right)\xi'+2\left(k''-k'\right)\xi\right]}{\left(1+4{\ell_c}^2(k+k'-2k'')^2\right)} \\
&\qquad-\frac{\sin\left[2(k-k')x-2\left(k-k''\right)\xi'-2\left(k''-k'\right)\xi\right]}{\left(1+4{\ell_c}^2(k-k')^2\right)} \\
&\qquad\left.-\frac{2\ell_c(k-k')\cos\left[2(k-k')x-2\left(k-k''\right)\xi'-2\left(k''-k'\right)\xi\right]}{\left(1+4{\ell_c}^2(k-k')^2\right)}\right\} \\
&\qquad\qquad\frac{2\left(k''-k'\right)\ell_c''v(\xi)f^{(0)}(k')v(\xi')}{\left(1+4\ell_c''^2\left(k''-k'\right)^2\right)}\,d\xi dk' d\xi' dk'',
\end{aligned}
\tag{47}
$$

where all integrations are taken from negative to positive infinity. The repeated integrals necessary to calculate this second order term make analytical expressions or simplifications untenable, so numerical techniques were used to elucidate the behavior of this next term of the series.

4.2 Numerical Integration of the Second Order Term

Theoretically, the form in Eq. (47), which resembles the form of the first order term in Eq. (45), could be included in simulation if the integrations are numerically evaluated each time boundary conditions are applied. In practice, however, this may be infeasible based on the considerable added computational burden this would contribute. To understand the nature of the second order term, Eq. (47) was integrated in the presences of a Dirac delta function in potential energy, that is where $v(x) = v_0\delta(x)$. Additionally, the boundary distribution is taken to be the Boltzmann distribution,

$$f^{(0)}(k) = e^{-\frac{\hbar^2 k^2}{2mk_BT}} = e^{-{\ell_h}^2 k^2}, \tag{48}$$

where l_h is a characteristic distance called the healing length. The Boltzmann distribution is an accurate description of the energetic distribution of electrons in low density scenarios, and it is reasonable to expect that results obtained in the low-density limit will hold at least qualitatively at higher densities.

These assumptions allow one to directly compare second order effects of perturbations in potential energy against the first order effects that Yoder was able to analytically calculate for situations of low electron densities. The form of the potential energy allows analytical evaluation of the remaining integrals over space, reducing Eq. (47) to

$$
\begin{aligned}
f^{(2)}(x,k) = \\
&\left(\frac{2\tau^2 v_0^2}{\pi^2\hbar^2}\right)\int_{-\infty}^{\infty}\int_{-\infty}^{\infty}\left\{\frac{2\ell_c(k+k'-2k'')\sin\left[2(k+k'-2k'')x\right]+\cos\left[2(k+k'-2k'')x\right]}{\left(1+4{\ell_c}^2(k+k'-2k'')^2\right)}\right. \\
&\qquad\left.-\frac{2\ell_c(k-k')\sin\left[2(k-k')x\right]+\cos\left[2(k-k')x\right]}{\left(1+4{\ell_c}^2(k-k')^2\right)}\right\} \\
&\qquad\qquad\frac{e^{-{\ell_h}^2k'^2}}{\left(1+4\ell_c''^2\,(k''-k')^2\right)}\,dk'dk'' \\
&+\left(\frac{2\tau^2 v_0^2}{\pi^2\hbar^2}\right)\int_{-\infty}^{\infty}\int_{-\infty}^{\infty}\left\{\frac{\sin\left[2(k+k'-2k'')x\right]+2\ell_c(k+k'-2k'')\cos\left[2(k+k'-2k'')x\right]}{\left(1+4{\ell_c}^2(k+k'-2k'')^2\right)}\right. \\
&\qquad\left.-\frac{\sin\left[2(k-k')x\right]+2\ell_c(k-k')\cos\left[2(k-k')x\right]}{\left(1+4{\ell_c}^2(k-k')^2\right)}\right\} \\
&\qquad\qquad\frac{2\,(k''-k')\,\ell_c''e^{-{\ell_h}^2k'^2}}{\left(1+4\ell_c''^2\,(k''-k')^2\right)}\,dk'dk''.
\end{aligned}
\tag{49}
$$

The integrand of the Eq. (49) contains oscillatory functions with k-space frequency of x/π. To resolve the numerical integration in respect to k' and k'' with sufficient accuracy, the integrand must be sampled to accurately capture these oscillations that additionally decay with k' due to the Boltzmann distribution. At large values of position, the regime where boundary conditions would ideally be applied, the discretization necessary to resolve these oscillatory functions can require considerable computational resources. Because of the high degree of resolution required for numerical evaluation of $f^{(2)}(x,k)$, the integration code was written in C++ and parallelized using the Message Passing Interface (MPI) to communicate between processors. The computation was completed on 32 AMD Opteron processors with 64 GB of RAM.

4.3 Numerical Results

In the upwinded discretization scheme, the relevant boundary values are located at negative wave vector for positive position and positive wave vector for negative position, so this discussion focuses on that domain. All results assume an effective mass of $0.0667m_0$ and a temperature of 77 K. Additionally, the integration over ξ is approximated by assuming a square potential barrier of height 1 eV and width 1 nm, so v_0 in Eq. (49) is the product of these two values.

Figure 4 shows the k-space calculation of the second order term with a relaxation time of 0.1 ps at 3, 6, 9, and 12 healing lengths away from the perturbation in potential energy at $x = 0$. The second order term behaves similarly to the first order term in wave vector as decaying oscillations can clearly be noted. As expected, the magnitude of the term decreases with increasing position away from the potential energy spike. This is an important feature in the application of boundary conditions in the WTE because the magnitude of $f^{(1)}(x, k)$ and $f^{(2)}(x, k)$ must be small in order for an approximate boundary value to be an accurate description of the true boundary condition. Since both leading order terms decay with separation distance from the delta in potential energy, an approximate boundary condition will be more accurate as the simulation boundary is placed farther from potential energy features used to design quantum mechanical devices.

In the low density limit, the spatial decay of the first order term was analytically shown to decay exponentially with the square of separation distance by a factor of the healing length in the asymptotic limit as $|x| \to \infty$ [26]. The limit where this asymptotic limit is reached in practice is increased at low values of wave vector through the introduction of finite values of the relaxation time τ. The second order term is also sensitive to the relaxation time chosen, as is evident in Figure 5 where the relaxation time τ is chosen to be 10 ps. The spatial decay appears to be much less pronounced at larger tau. Since the WDF will relax to known distributions

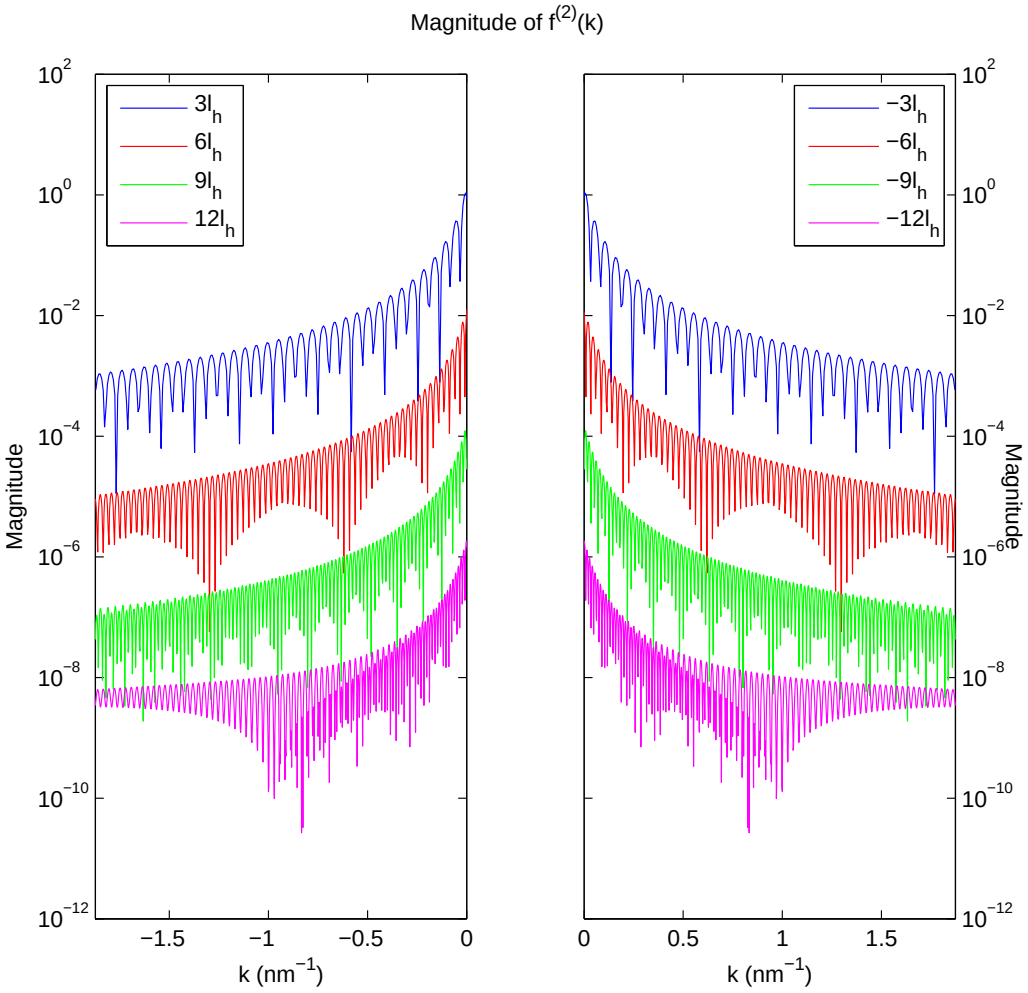

Figure 4: The second order term was calculated with $\tau = 0.1\,\text{ps}$. It exhibits similar k-space behavior as the first order term with rapid oscillations and a decaying envelope. The envelope function is monotonically decreasing in position as was the case with this first error term. This implies that the error caused by an approximate boundary condition can be minimized by increasing the separation distance between the boundary and features in the potential energy profile.

through scattering processes described by the relaxation time, it follows that the error in the boundary condition should be sensitive to τ because it takes relatively longer distances for electrons to relax to the distributions being used to approximate the boundary value. This means that at higher relaxation times, larger separation distances are required between boundaries and potential energy device structures to have meaningful results.

It is imperative to determine at what distance successive terms in the asymptotic series in Eq. (44) are smaller in magnitude than previous terms in order for it to be useful for correcting boundary values. This point will provide insight into the choice of locations for application of approximate boundary conditions. Figure 6 compares the magnitudes of the first and second order terms for a relaxation time of 0.1 ps. For the specific conditions of this calculation, the magnitude of the second order term is higher than that of first order term, and this continues to be true for increasing position. Although an analytic form of the asymptotic solution as $|x| \to \infty$ is known for $f^{(1)}(x,k)$ [26], the asymptotic form of $f^{(2)}(x,k)$ is not known analytically. Clear from these results, however, is that the behavior of the second order term, is influenced by both scattering and perturbations in potential energy. Further analysis is necessary to determine the asymptotic form of the spatial decay of the second order term analytically, and establish the relative influences of $f^{(1)}(x,k)$ and $f^{(2)}(x,k)$ on fundamental quantities such as electron density, current density, energy density, etc.

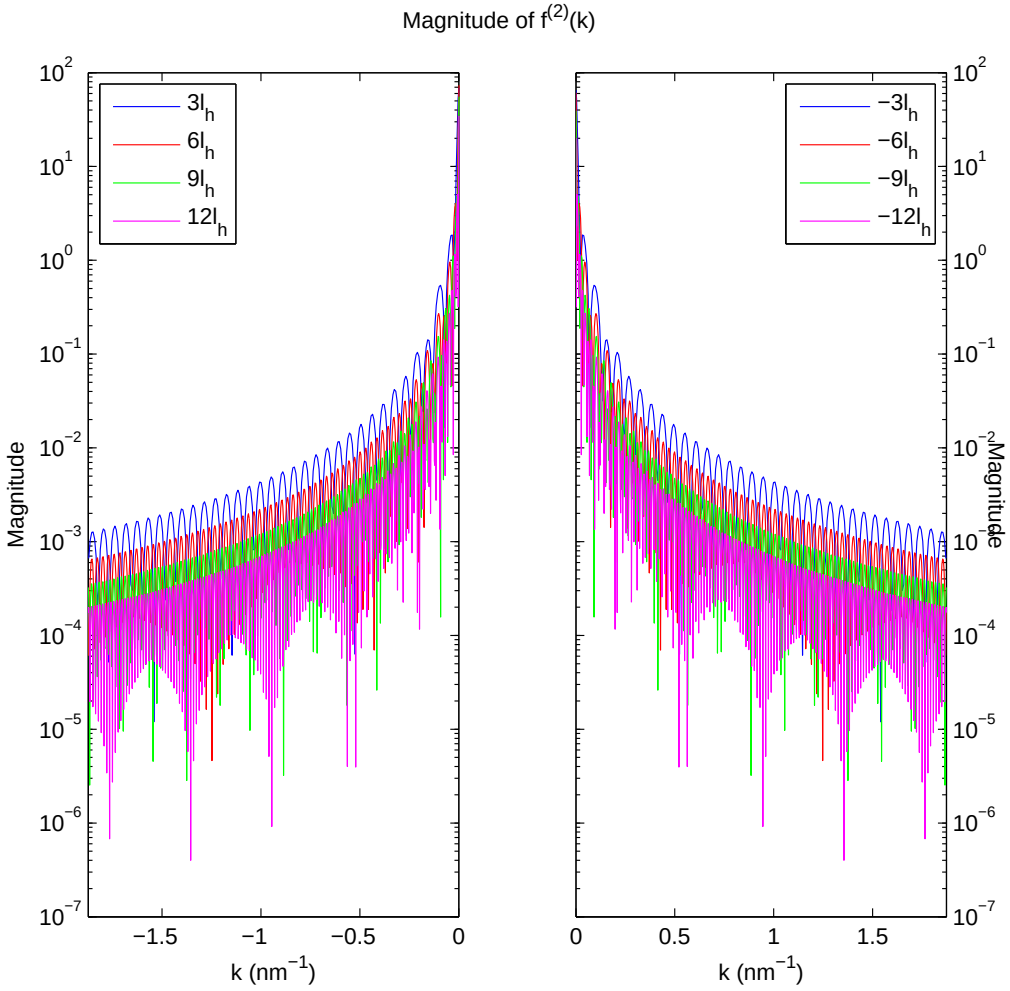

Figure 5: As the relaxation time is increased to 10 ps and the transport becomes more coherent, the second order error decays much slower in position. Therefore, approximate boundary conditions must be applied farther away from the active region of a device simulation at large τ.

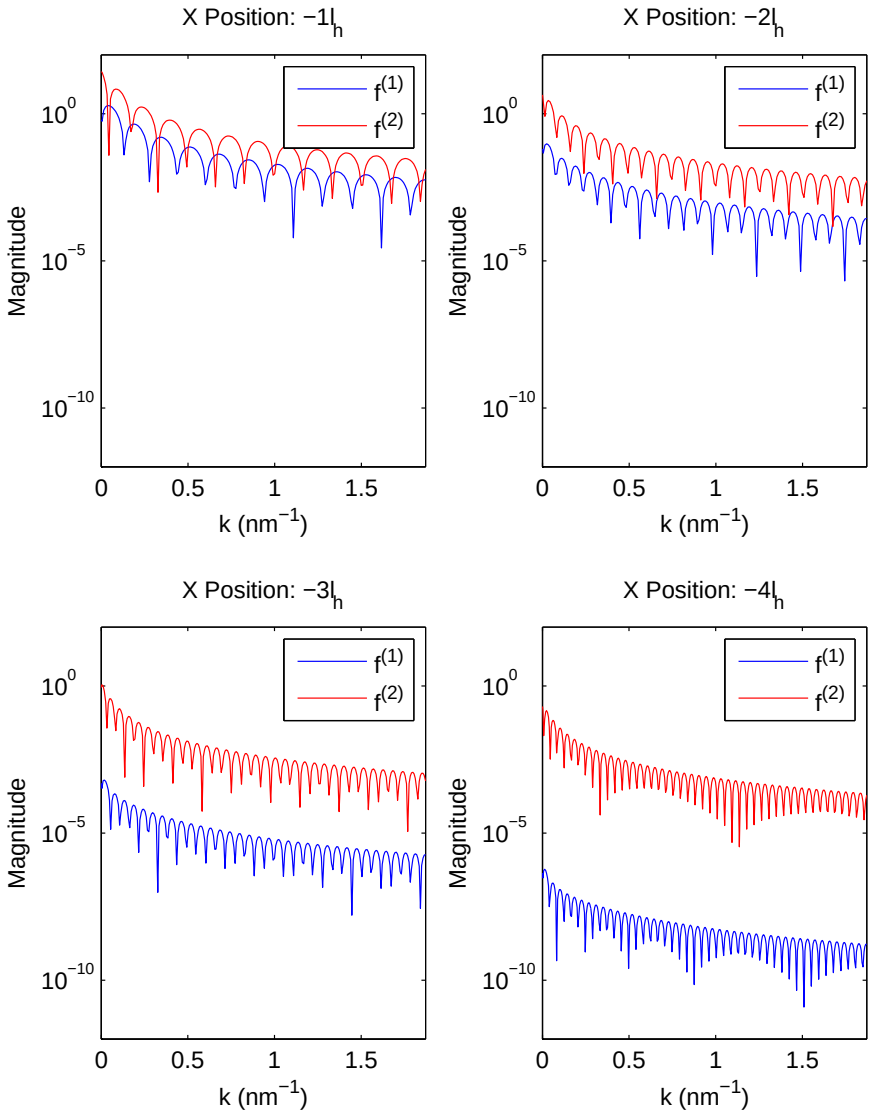

Figure 6: With a relaxation time of 0.1 ps, the second order term of the series is larger than the first order term for all tested positions.

CHAPTER V

NUMERICAL DISCRETIZATION OF FIRST ORDER CORRECTION TERM

Since the typical position-independent boundary conditions are only an approximation, inclusion of the first order term of Eq. (44) may improve simulation accuracy. Including the first order correction into simulation requires the computed value to be self-consistently solved with the WTE and Poisson's equation, so the equations necessary to include the first error term into simulation are developed.

Incorporating the first order term into the four-point discretization scheme described previously takes care because the correction terms in Eq. (44) are position-dependent. For example, the equations for the leftmost position node of the discrete WTE in Eq. (35) for $j = 0$ can be written as

$$\begin{aligned}&\frac{\hbar k_\ell}{2m\Delta x}\left[f_{-2,\ell} - 4f_{-1,\ell} + 3f_{0,\ell}\right] + \frac{1}{\tau}f_{0,\ell} - \frac{1}{\tau}f^{(0)}(k_\ell)\\ &-\frac{\Delta x \Delta k}{\pi\hbar}\sum_m\sum_p\left\{\sin\left(\left(k_\ell - k_p\right)\xi_m\right)\left[v\left(x_0 + \frac{\xi_m}{2}\right) - v\left(x_0 - \frac{\xi_m}{2}\right)\right]\right\} f_{0,p} = 0,\ k_l > 0,\end{aligned} \tag{50}$$

where $f_{-2,\ell}$ and $f_{-1,\ell}$ refer to the boundary values of the function outside the simulation domain. These two boundary nodes are traditionally taken to be described by some position-independent expression such as Eq. (39) and can thus be taken as the same value. The addition of the any correction terms, however, necessitates the consideration of the position of each boundary node as is shown in Figure 7.

The addition of the first-order correction term also requires careful implementation into Newton's method to calculate the stationary WDF. Eq. (45) has a functional

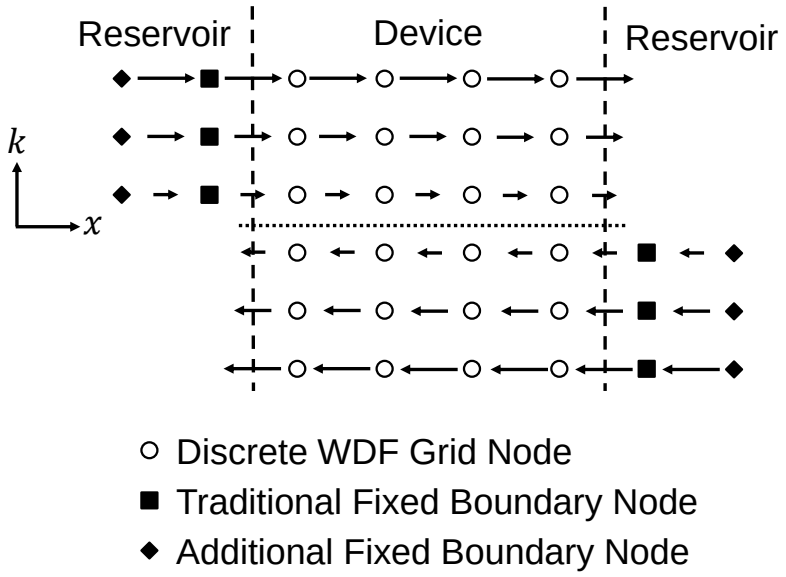

Figure 7: The discretization scheme for the Wigner transport equation has fixed boundary values outside the device domain. Traditionally, the boundaries depicted as solid black squares are not functions of position and can be thought of as just outside the simulation domain. The addition of correction terms introduces a functional dependence on position, and thus additional boundary values depicted as solid black diamonds must be explicitly considered. Adapted from [8].

dependence on both the electrostatic potential ϕ through the the potential energy and the drift parameter δk. Therefore, derivatives with respect to both of these solution variables must be included into the equations that contain the boundary values, which, in the upwind differencing scheme used, are all equations for the leftmost two and rightmost two spatial nodes.

The derivative of Eq. (45) in respect to the drift parameter can be expressed as

$$\frac{\partial f^{(1)}(x_j,k_\ell)}{\partial(\delta k)} = \frac{2\tau\Delta x\Delta k}{\pi\hbar}\sum_m\sum_p \frac{\sin\left(2\left(k_\ell-k_p\right)\left(x_j-\xi_m\right)\right)}{1+4\left(k_\ell-k_p\right)^2{\ell_c}^2} v(\xi_m)\left.\frac{\partial f^{(0)}}{\partial(\delta k)}\right|_{k_p} - \frac{2\tau\Delta x\Delta k}{\pi\hbar}\sum_m\sum_p \frac{2\left(k_\ell-k_p\right)\ell_c\cos\left(2\left(k_\ell-k_p\right)\left(x_j-\xi_m\right)\right)}{1+4\left(k_\ell-k_p\right)^2{\ell_c}^2} v(\xi_m)\left.\frac{\partial f^{(0)}}{\partial(\delta k)}\right|_{k_p} \quad (51)$$

$$\left.\frac{\partial f^{(0)}}{\partial(\delta k)}\right|_{k_p} = \frac{(k_p-\delta k)}{\pi}\frac{e^{-\frac{\hbar^2(k_p-\delta k)^2}{2mk_BT}+\frac{\mu}{k_BT}}}{1+e^{-\frac{\hbar^2(k_p-\delta k)^2}{2mk_BT}+\frac{\mu}{k_BT}}}. \quad (52)$$

Incorporation of this term is the simpler of the two derivatives necessary because it only is added to the one column of the Jacobian matrix used in the Newton iterations that refers to the δk calculation.

The derivative of Eq. (45) in respect to the electrostatic potential has a slightly simpler form given as

$$\frac{\partial f^{(1)}(x_j,k_\ell)}{\partial\phi(\xi_m)} = -\frac{2q\tau\Delta x}{\pi\hbar}\sum_m \frac{\sin\left(2\left(k_\ell-k_p\right)\left(x_j-\xi_m\right)\right)}{1+4\left(k_\ell-k_p\right)^2{\ell_c}^2} f^{(0)}(k_p) + \frac{2q\tau\Delta x}{\pi\hbar}\sum_m \frac{2\left(k_\ell-k_p\right)\ell_c\cos\left(2\left(k_\ell-k_p\right)\left(x_j-\xi_m\right)\right)}{1+4\left(k_\ell-k_p\right)^2{\ell_c}^2} f^{(0)}(k_p) \quad (53)$$

Note that this derivative applies to the equation referring to the x node x_j and k node k_ℓ but is in respect to the electrostatic potential at a different position ξ_m. Therefore, this term must be calculated for each column of the Jacobian matrix that refers to the electrostatic potential within a correlation length resulting in multiple additions for each row incorporating a boundary value. Since, however, entries already exist at these matrix indices, the overall structure of the matrix in not altered.

CHAPTER VI

CONCLUSION

Simulations using the Wigner transport equation have shown to be effective at accurately predicting the operation of many electronic devices that exhibit quantum effects. The nonlocal nature of quantum mechanics, however, forces models to incorporate approximate boundary conditions, which can be the source of inaccurate and unphysical results. To address this issue, the Yoder group has developed an asymptotic series to quantitatively evaluate the error incurred via the application of approximate boundary conditions.

In this thesis, the nature of the series is investigated by calculating the second term of this series and presenting an expression that could be used in simulation to include second order effects. Calculation of second order effects, however, requires considerable computational resources due to the repeated integrals necessary. Numerical investigations of second order effects show that the second order term exhibits behavior similar to that of the first order term in that it is oscillatory in wave vector and decays with position away from perturbations in potential energy. Like the first order term, the decay envelope of the the second order term is a function of the relaxation time. Larger relaxation times cause the envelope to decay more slowly with increasing position. For the specific case studied and the range of standoff distances considered, comparison of first and second order terms show that the second order term is greater than the first order term, though an analytic expression for the asymptotic behavior of the second order term has yet to be derived. In addition to analysis of the second order term, the methodology to incorporate the first order correction term into a steady-state Wigner transport simulation that relies on Newton's method

for self-consistency is presented.

More work is needed, however, to ascertain the asymptotic form of the second order term in the expansion in order to assess the error associated with zeroth or first order approximate boundary conditions. Because this work has shown that the relaxation time is an important parameter in the decay behavior of the second order term, future work could entail using multi-scale perturbation theory to characterize how the potential energy and the relaxation time both affect the second order term. Other future work involves simulating electronic devices with and without error terms to characterize the effect on the accuracy of simulations and demonstrate error correction.

REFERENCES

[1] Abramowitz, M. and Stegun, I. A., *Handbook of mathematical functions: with formulas, graphs, and mathematical tables*. Courier Dover Publications, 2012.

[2] Bertoni, A. and Bordone, P., "The Wigner function for electron transport in mesoscopic systems," *Journal of Physics: Condensed Matter*, vol. 11, no. 31, pp. 5999–6012, 1999.

[3] Biegel, B., *Quantum electronic device simulation*. PhD thesis, Stanford University, 1997.

[4] Bourgade, J. and Degond, P., "Quantum corrections to semiclassical transport in nanoscale devices using entropy principles," *Journal of Computational Electronics*, vol. 6, no. 1, pp. 117–120, 2007.

[5] Buot, F. A. and Jensen, K. L., "Lattice Weyl-Wigner Formulation of exact many-body quantum-transport theory and application to novel solid-state quantum-based devices," *Physical Review B*, vol. 42, no. 15, 1990.

[6] Case, W. B., "Wigner functions and Weyl transforms for pedestrians," *American Journal of Physics*, vol. 76, no. 10, p. 937, 2008.

[7] Ferry, D. and Grubin, H., "Modeling of quantum transport in semiconductor devices," *Solid State Physics*, vol. 49, pp. 283–448, 1996.

[8] Frensley, W. R., "Wigner-function model of a resonant-tunneling semiconductor device," *Physical Review B*, vol. 36, pp. 1570–1580, July 1987.

[9] Frensley, W. R., "Boundary conditions for open quantum systems driven far from equilibrium," *Reviews of Modern Physics*, vol. 62, pp. 745–791, July 1990.

[10] Jensen, K. and Buot, F., "The methodology of simulating particle trajectories through tunneling structures using a Wigner distribution approach," *IEEE Transactions on Electron Devices*, vol. 38, no. 10, pp. 2337–2347, 1991.

[11] Jiang, H. and Cai, W., "Effect of boundary treatments on quantum transport current in the Green's function and Wigner distribution methods for a nano-scale DG-MOSFET," *Journal of Computational Physics*, vol. 229, pp. 4461–4475, June 2010.

[12] Jiang, H., Cai, W., and Tsu, R., "Accuracy of the Frensley inflow boundary condition for Wigner equations in simulating resonant tunneling diodes," *Journal of Computational Physics*, vol. 230, pp. 2031–2044, Mar. 2011.

[13] Jiang, H., Lu, T., and Cai, W., "A device adaptive inflow boundary condition for Wigner equations of quantum transport," *Journal of Computational Physics*, vol. 258, pp. 773–786, Feb. 2014.

[14] Kluksdahl, N., Kriman, A., Ferry, D. K., and Ringhofer, C., "Self-consistent study of the resonant-tunneling diode," *Physical Review B*, vol. 39, no. 11, 1989.

[15] Lasater, M., *Numerical methods for the Wigner-Poisson equations*. PhD thesis, North Carolina State University, 2005.

[16] Rossi, F., Jacoboni, C., and Nedjalkov, M., "A Monte Carlo solution of the Wigner transport equation," *Semiconductor Science and Technology*, vol. 9, no. 5S, pp. 934–936, 1994.

[17] Sarker, S., Davies, J., Khan, F., and Wilkins, J., "Quantum corrections to the Boltzmann equation for transport in semiconductors in high electric fields," *Physical Review B*, vol. 33, no. 10, 1986.

[18] Savio, A. and Poncet, A., "Study of the Wigner function boundary conditions at different barrier heights," in *2010 International Conference on Simulation of Semiconductor Processes and Devices*, no. 2, pp. 163–166, Ieee, Sept. 2010.

[19] Schrödinger, E., "Quantisierung als eigenwertproblem," *Annalen der physik*, vol. 385, no. 13, pp. 437–490, 1926.

[20] Selberherr, S., *Analysis and Simulation of Semiconductor Devices*. Springer New York, 1984.

[21] Taj, D., Genovese, L., and Rossi, F., "Quantum-transport simulations with the Wigner-function formalism: Failure of conventional boundary-condition schemes," *Europhysics Letters (EPL)*, vol. 74, pp. 1060–1066, June 2006.

[22] Thompson, S. and Parthasarathy, S., "Moore's law: the future of Si microelectronics," *Materials Today*, vol. 9, pp. 20–25, June 2006.

[23] Tsu, R. and Esaki, L., "Tunneling in a finite superlattice," *Applied Physics Letters*, vol. 22, no. 11, pp. 562–564, 1973.

[24] Wigner, E., "On the quantum correction for thermodynamic equilibrium," *Physical Review*, vol. 40, pp. 749–759, 1932.

[25] Yoder, P. D., Grupen, M., and Smith, R. K., "Demonstration of Intrinsic Tristability in Double-Barrier Resonant Tunneling Diodes With the Wigner Transport Equation," *IEEE Transactions on Electron Devices*, vol. 57, no. 12, pp. 3265–3274, 2010.

[26] Yoder, P. D. Private Communication, 2013.